Carbon 126 (2018) 128–134

Contents lists available at ScienceDirect

Carbon

journal homepage: www.elsevier.com/locate/carbon

Graphene structure boosts electron transfer of dual-metal doped carbon dots in photooxidation

Qinggang Zhang, Wenming Xu, Congcong Han, Xiaokai Wang, Yixian Wang, Zhongtao Li, Wenting Wu*, Mingbo Wu

State Key Laboratory of Heavy Oil Processing, School of Chemical Engineering, China University of Petroleum, Qingdao 266580, People's Republic of China

ARTICLE INFO

Article history:
Received 1 August 2017
Received in revised form
18 September 2017
Accepted 3 October 2017
Available online 5 October 2017

ABSTRACT

Carbon dots as a novel photocatalyst have attracted much attention, but they are still limited by their poor electron transfer properties. It is worth noting that graphene structures as a major component of carbon dots, play an important role in the electron transfer properties and photocatalysis. Herein, under different calcination temperature, carbon dots with various graphitization degrees were prepared from the mixture of EDTA-Fe and EDTA-Cu via a facile one-step pyrolysis. The graphitization degree of FeCu-CDs was proved by means of Raman, XRD and XPS spectra. The FeCu-CDs prepared at high temperature have higher graphitization degree and show excellent electron transfer ability. On the other hand, unsaturated metal dopants with mixed valence states (Fe^{2+}, Fe^{3+}, Cu^{+} and Cu^{2+}) were fabricated and proved by XPS, ESR and FT-IR spectra, which are beneficial to further enhance both the electron donating/accepting abilities by changing their valence state. This higher graphitization degree and its synergy with dual metal dopants in FeCu-CDs can promote the photocatalytic efficiency in the photooxidation reaction of 1,4-DHP.

1. Introduction

The development and exploration of renewable and abundant solar energy have attracted widespread attention [1–7]. In this regard, much efforts have been devoted to the exploration of efficient and low cost photocatalyst for solar energy conversion and energy storage [8,9]. Fortunately, carbon dots (CDs), as a relatively new class of nano carbon materials, have broadband absorption ability and abundant functional groups, and they show great potential in the field of photocatalysis [10,11]. For the photocatalysis, they have three key factors: broadband absorption ability, excellent electron transfer and proper photoredox properties [12]. There is still much room left for the improvement of the CDs' properties mentioned above, especially for the electron transfer. Based on the CDs' structure, its electron-transfer improvement could be mainly divided into two parts: CDs' surface and their interior structure. Sun et al. utilized surface attachment with oligomeric ethylene glycol diamine (PEG) to enhance the electron transfer [13]. We have also reported the modification with strong surface groups to improve the electron transfer properties of CDs derived from raw materials (petroleum coke) [14]. For the improvement of CDs' interior structure, Cu–N dopants in CDs were designed to enhance both electron donating and accepting abilities [15]. Actually, graphene structure is an important component for most CDs' interior structure, which cannot be neglected in the improvement of electron transfer properties.

Graphene has exceptional electronic and optical properties, and to some extent, the graphene degree could strongly influence CDs' electron transfer properties [16–19]. In the metal doping CDs system, graphene is the major component, and it could act as a ligand to chelate with metal in the metal doping CDs system [15]. After irradiation, the graphene may easily accept the photo energy, and promote the electron transfer to the metal dopants through its own pathway. In another point of view, the metal dopants' properties, such as valence state, may change during this process, and it may provide a unique electron transfer pathway for the photocatalysis [20–23]. Moreover, the presence of graphene structure could enhance the extension of light absorption range, the intensity of absorbed light, and chemical stability of photocatalyst [24].

Herein, through a facile one-step pyrolysis, dual-metal doped CDs (FeCu-CDs) with different graphene degree were prepared from the mixture of EDTA-Fe and EDTA-Cu under various

* Corresponding author.
E-mail address: wuwt@upc.edu.cn (W. Wu).

https://doi.org/10.1016/j.carbon.2017.10.006
0008-6223/

temperature. It provides an insight into the synergy effect of graphene on the metal dopants and photooxidation. The graphene structure and its degree were carefully studied by TEM, Raman, XRD and XPS spectra. With the assistance of graphene structure, the metal dopants in FeCu-CDs come to mixed valence states (Fe^{2+}, Fe^{3+}, Cu^{+} and Cu^{2+}), which were confirmed by X-ray photoelectron (XPS) spectroscopies, FT-IR spectra and Electron spin resonance (ESR). With optimized pyrolysis temperature and mass ratio of EDTA-Fe and EDTA-Cu, the higher graphitization degree and its synergy with metal dopants in FeCu-CDs could enhance the electron transfer abilities and promote extraordinarily high activity for the photooxidation of 1,4-dihydro-2,6-dimethylpyridine-3,5-dicarboxylate (1,4-DHP), which is the key component in various bioactive compounds and a good substrate for the production of pyridine derivatives [25,26]. And pyridine derivatives have found applications in various fields such as in the synthesis of drugs, herbicides, or insecticides [27–29]. The conversion of 1,4-DHP catalyzed by FeCu-CDs is 8 times higher than that of pure CDs. A possible mechanism of the photocatalytic reaction process was proposed based on the measurements of ESR signal of metal dopants and superoxide anion radical ($O_2^{-\bullet}$) at different irradiation time.

2. Experimental

2.1. Chemicals

Ethylenediaminetetraacetic acid ferric sodium salt (EDTA-Fe), ethylenediaminetetraacetic acid copper disodium salt (EDTA-Cu) and ethylenediaminetetraacetic acid disodium salt (EDTA-Na) were purchased from Liaoyang Wan Rong Chemical products Co., Ltd., China. All chemicals were directly used without further purification in our experiments.

2.2. Preparation of 350-FeCu-CDs

Typically, the CDs were prepared via a facile one-step pyrolysis that has been reported by our group before [15]. A quartz boat filled with EDTA-Fe and EDTA-Cu (the mass ratio was 1:2, 1:1 and 2:1 named 350-FeCu-CDs-1, 350-FeCu-CDs-2 and 350-FeCu-CDs-3) was put into the center of a quart tube, and calcined in a tube furnace at 350 °C for 2 h at a heating rate of 5 °C/min under flowing N_2 atmosphere. When the temperature is higher than 350 °C, the polymerization degree is too high to form FeCu-CDs in the nanoscale, resulting instead in the formation of powders on the microscale. So the 350 °C was selected as the highest reaction temperature. The collected target product was grinded and dissolved in water (150 mL), and the mixture was processed by the ultrasonic treatment for 20 min at room temperature. The pretreated product was filtered with slow-speed quantitative millipore filter (0.22 μm) to remove insoluble substance. After filtering process, the solution was dialyzed with MD34 (3500 Da) dialysis tube for 48 h to remove the remaining salts and small fragments. The solution was dried at 60 °C and 350-FeCu-CDs powder was obtained. The dual metal doping CDs are referred to as 350-FeCu-CDs. In the following introduction, the CDs (Fe: Cu = 1:2) was named as 350-FeCu-CDs uniformity if there is no special description.

Single metal doping CDs was prepared using only EDTA-Fe or EDTA-Cu at 350 °C named Fe-CDs and Cu-CDs. Meanwhile, no metal doping CDs was prepared using EDTA-Na, the product was named as Na-CDs.

2.3. Preparation of 250-FeCu-CDs

The mixture of EDTA-Fe and EDTA-Cu (the mass ratio was 1:2, 1:1 and 2:1 named 250-FeCu-CDs-1, 250-FeCu-CDs-2, 250-FeCu-CDs-3) was calcined at 250 °C for 2 h at a heating rate of 5 °C/min under N_2 atmosphere. Other experiments conditions were unchanged. The CDs (Fe: Cu = 1:2, 250 °C) was named as 250-FeCu-CDs uniformity.

2.4. Photooxidation of 1,4-DHP

Photooxidation was carried out according to a modified literature method [15]. 1,4-DHP, an organic substance, can be dissolved in the mixture of ethanol and water, wherein ethanol could dissolve 1,4-DHP and water could reduce the cost of photooxidation. An ethanol/water (1:1 v/v, 20 mL) mixed solvent containing 1,4-DHP (1.0×10^{-4} M) and the photosensitizer (CDs, 0.15 mg/mL) was put into a round bottom flask (50 mL). The solution was then irradiated using a xenon lamp with a power of about 35 W (600 W m^{-2}, $\lambda > 385$ nm) through a cutoff filter (0.72 M $NaNO_2$ solution, which can filter the wavelength of $\lambda < 385$ nm). UV–Vis absorption spectra were used to record at intervals of 10 min. The consumption of 1,4-DHP was monitored by a decrease in the absorption at 374 nm.

2.5. Samples characterization

Transmission electron micrographs (TEM) images were taken on a JEOL JEM-2100UHR microscope with an accelerating voltage of 200 kV. X-ray powder diffraction (XRD) was obtained by using PANalytical X-ray Diffractometer equipped with Cu Kα radiation ($\lambda = 0.15406$ nm, 40 kV, 40 mA). Further evidence for the composition of the product was inferred from X-ray photoelectron spectroscopy (XPS), using ESCALAB 250Xi spectrometer equipped with Al X-ray source. Fourier transform infrared (FT-IR) spectra were recorded on a Nicolet 6700 spectrometer. Raman spectra measurement was carried out by using Raman Microscopy (Horiba, LabRAM HR Evolution, France) with an excitation wavelength of 532 nm. The Fe and Cu contents in the FeCu-CDs were measured by atomic absorption spectroscopy (AAS, contr AA700), which was produced by Analytikjena. UV–Vis absorption spectra were measured by a UV–Vis spectrophotometer (UV-2700, SHIMADZU). Fluorescence spectra were measured by a spectrofluorometer (F-97 Pro, Shanghai Lengguang Technology Co., Ltd., China). Electron spin resonance (ESR) spectra were recorded at room temperature using a JEOL JES FA200 spectrometer at 9.8 GHz, X-band, with 100 Hz field modulation. Samples were quantitatively injected into specially made quartz capillaries for ESR analysis in the dark and illuminated directly in the cavity of the ESR spectrometer. All optical measurements were performed at room temperature.

3. Results and discussion

3.1. Structural characterization of FeCu-CDs

The morphology and structure of 350-FeCu-CDs were firstly studied as shown in Fig. 1a and Fig. S1. 350-FeCu-CDs are monodisperse and uniform, and the average diameters of the 350-FeCu-CDs are about 4.2 nm. High-resolution TEM (HRTEM) image (inset image in Fig. 1a) exhibits a good crystallinity of 350-FeCu-CDs with a lattice spacing of 0.2 nm which could be attributed to the lattice fringes of the (100) plane of graphite carbon [30–32]. XRD patterns of 350-FeCu-CDs and 250-FeCu-CDs were shown in Fig. S2a. There is a diffraction peak at 25.5° which is the characteristic peak of carbon corresponding to the (002) plane of graphitic carbon [30]. Compared with 250-FeCu-CDs, the peak of 350-FeCu-CDs is narrower indicating that 350-FeCu-CDs has higher graphitization degree [33]. Fig. S2b reveals the Raman spectra of 350-FeCu-CDs and

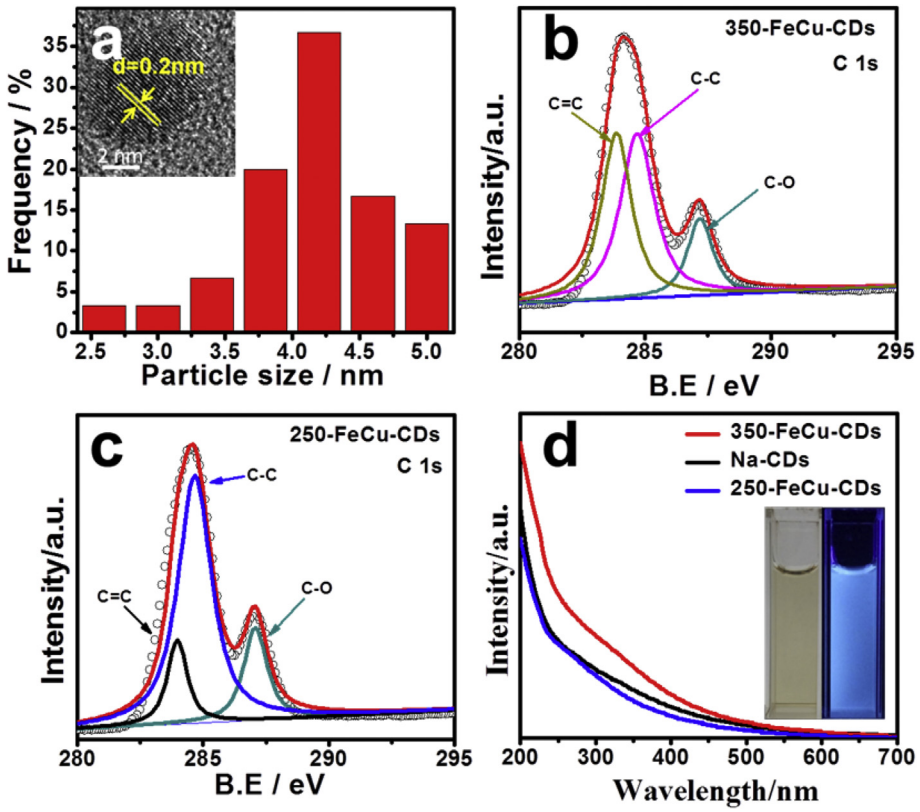

Fig. 1. (a) The size distribution of 350-FeCu-CDs and HRTEM (inset) image of 350-FeCu-CDs; (b) XPS C 1s spectrum of 350-FeCu-CDs; (c) XPS C 1s spectrum of 250-FeCu-CDs; (d) UV–Vis absorption spectra of CDs solution, inset: photographs of 350-FeCu-CDs in daylight (left) and UV-light irradiation, λex = 365 nm (right). (A colour version of this figure can be viewed online.)

250-FeCu-CDs with typical D and G bands of carbon materials observed. The peak at 1360 cm^{-1} (D band) is associated with the vibrations of sp3-carbon atoms in disordered graphite, and the peak at 1570 cm^{-1} (G band) corresponds to the vibration of sp2 hybrid carbon atoms [34]. The ratio of these two peaks (I_D/I_G) indicates the level of the graphitization degree, thus the smaller value has the higher the degree of graphitization. For 350-FeCu-CDs, its I_D/I_G ratio could come to 0.76 which is lower than that of 250-FeCu-CDs (0.93). These results indicate that 350-FeCu-CDs have higher graphitization degree [34].

To further confirm the composition of FeCu-CDs, Fourier transform infrared (FT-IR) spectra and X-ray photoelectron spectroscopy (XPS) of FeCu-CDs were investigated. For the FT-IR spectra (Fig. S2c), the typical band at 3412 and 1107 cm^{-1} are assigned to –OH group and C–O stretching vibration which could greatly improve aqueous solubility of the CDs [35,36]. And the peaks at 2942, 1628 and 1372 cm^{-1} could be attributed to the Ar–H of aromatic hydrocarbon, the C=C and C=N/C–N in-plane stretching vibrations of amino groups [35,36]. XPS spectra were used to further study the percentage of these functionalized groups (Fig. 1b–c, Figs. S3 and S4). FeCu-CDs mainly contain C, N, O, Fe and Cu elements. The high resolution C1s XPS spectra (Fig. 1b and c) could be divided into three characteristic peaks of C=C, C–C, C–O (283.9, 284.7 and 287.3 eV) [14,37]. For the 350-FeCu-CDs, the percentage of aromatic C=C could come to 39.6 at%, which is higher than that of 250-FeCu-CDs (13.8 at%). This result is consistent with those of FT-IR, Raman, and XRD, indicating that 350-FeCu-CDs have higher graphitization degree. The high resolution N1s XPS spectrum (Fig. S3a) of 350-FeCu-CDs shows characteristic peaks of pyridinic N, amine moieties (or other sp^3-C and nitrogen bonds), pyrrolic N and graphitic N at 398.6 eV, 399.3 eV, 400.0 eV and 401.4 eV, respectively [38,39]. However, the high resolution N1s XPS spectrum (Fig. S4a) of 250-FeCu-CDs lacks the graphitic N. It indicates that the graphitic N could be formed at high temperatures and the introduction of graphitic N can increase the conductivity of the CDs to some extent.

The spectra properties were also studied here. Fig. 1d shows the UV–Vis absorption spectra of these CDs, revealing a broadband absorption from 200 to 700 nm. As confirmed by the atomic absorption spectrometry (Table S1), the Fe and Cu contents in 250-FeCu-CDs are 2.9% and 3.0%, respectively. They are higher than those of 350-FeCu-CDs (Fe: 0.4% and Cu: 2.3%). However, compared with no metal doping CDs (Na-CDs), Fe/Cu doped CDs prepared at low temperature (250-FeCu-CDs) show a little weaker absorption intensity. It indicates that the metal-doping content is not the crucial factor for enhancing the absorption intensity. The relative stronger intensity of Na-CDs may be attributed to the larger π conjugation from the graphene structure. On another hand, 350-FeCu-CDs show stronger absorption intensity than that of Na-CDs and 250-FeCu-CDs, which could be assigned to the efficient electron transfer from metal dopants to the graphene structure. It indicates that the higher temperature induced graphene structure benefits both the absorption intensity and electron transfer mentioned above. The solution of 350-FeCu-CDs gives bright blue-green emission (the inset image in Fig. 1d). 350-FeCu-CDs show excitation-dependent emission (Fig. S5). As the excitation wavelengths changes from 320 nm to 460 nm, the emission spectrum of 350-FeCu-CDs exhibits a gradual red-shift phenomenon, which is consistent with the results reported before [36].

To some extent, these graphene structures promote the formation of unsaturated metal dopants, which were carefully analysed by ESR, FT-IR and XPS spectra. FeCu-CDs were firstly measured by

ESR spectra (Fig. 2a). For Cu signal, the g value of Cu is 2.09, which is less than 2.30 [15]. It indicates that Cu^{2+} covalently chelated with the surrounding graphene structure in CDs. For Fe signal, the g value of Fe is 4.22, corresponding to Fe^{3+} in CDs [40]. Unfortunately, Fe^{2+} and Cu^{1+} cannot be detected by ESR. But the FT-IR spectrum of FeCu-CDs confirms the existence of Cu^{+}, and its stretch absorption is observed at 647 cm^{-1} (Fig. 2b) [41]. Fortunately, XPS could provide relatively comprehensive analysis for the unsaturated metal dopants. As shown in Figs. S3c and S4c, the XPS spectra of the Fe 2p have the Fe^{2+} peak at 709.0 and 722.7 eV and the Fe^{3+} peak at 711.1 eV and 724.6 eV [42]. The Cu 2p peak can be divided into four different peaks located at 932.4 eV (Cu^{+}), 933.4 eV (Cu^{2+}), 952.3 eV (Cu^{+}) and 952.8 eV (Cu^{2+}) (Figs. S3d and S4d) [43–45]. For the 350-FeCu-CDs, the percentage of Cu^{+} (75.9 at%) and Fe^{2+} (39.5 at%) is higher than those of 250-FeCu-CDs (Cu^{+} 63.5 at% and Fe^{2+} 38.0 at %). With the help of the surrounding graphene structure, these unsaturated metal dopants would be beneficial to enhance both the electron donating and accepting abilities.

3.2. Electron transfer properties of FeCu-CDs

Excellent electron donating and accepting abilities are key factors for CDs' potential applications in the light energy conversion [13]. Electron acceptor 2,4-dinitrotoluene (DNT) and electron donor *N,N*-diethylaniline (DEA) are usually used as fluorescence quenching agent to measure the electron donating and accepting abilities of CDs. The Stern–Volmer plots, in which the integrated emission intensity was plotted versus the quencher concentration (DNT: 0–0.003 M, DEA: 0–0.03 M), were assisted in analyzing the emission quenching (Fig. 3a–b) [15].

For the electron donating abilities of CDs, the emission intensity was quenched by adding different concentrations of DNT as shown in Fig. S6 and Fig. 3a. The Stern–Volmer quenching constants (*K*sv) for 350-FeCu-CDs, Fe-CDs, Cu-CDs and 250-FeCu-CDs are 564.36 M^{-1}, 265.30 M^{-1}, 207.07 M^{-1} and 139.32 M^{-1}, respectively. Compared with 250-FeCu-CDs, the electron donating ability of 350-FeCu-CDs was increased 4.1-fold, which could be attributed to higher graphitization degree at 350 °C. The electron donating ability of 350-FeCu-CDs was also higher than that of Fe-CDs and Cu-CDs, which may be due to synergistic effects of Fe and Cu species in CDs. The same results could be obtained for their electron accepting ability. The Stern–Volmer quenching constants (*K*sv) for 350-FeCu-CDs, Fe-CDs, Cu-CDs and 250-FeCu-CDs are 13.92 M^{-1}, 10.64 M^{-1}, 10.54 M^{-1} and 7.09 M^{-1}, and the electron accepting ability of 350-FeCu-CDs was approximately 2.0-fold higher than that of 250-FeCu-CDs (Fig. 3b and Fig. S7). The electrochemical impedance spectroscopy (EIS) further demonstrates the electron transfer ability of CDs (Fig. S8). 350-FeCu-CDs show smaller diameter of Nyquist circle than that of 250-FeCu-CDs and Na-CDs, namely 350-FeCu-CDs has lower charge transfer resistance. These results show that the synergetic effect of dual-metal doped and higher graphitization degree can improve both the electron donating and accepting abilities, which are beneficial to their application in next photooxidation reactions.

3.3. Photooxidation activities

In order to further verify the electron transfer ability of carbon dots, photocatalytic oxidation of 1,4-DHP was tested, which is a typical electron transfer process of the photocatalytic reaction [14,15]. In order to compare the photocatalytic abilities of different CDs, the photooxidation of 1,4-DHP was carried out (Fig. S9a), which was irradiated under air atmosphere and was characterized by UV–Vis absorption spectra. By irradiating the mixed solution of FeCu-CDs and 1,4-DHP with a xenon lamp (35 W) for 100 min, the absorption of 1,4-DHP at 374 nm decreased and the absorption of the product (pyridine derivative) at 280 nm increased, respectively (Fig. S9b-c). Under the same reaction condition, the conversions of 1,4-DHP were listed in Table S2, Fig. S9 and Fig. 3c. For 350-FeCu-CDs, the conversion of 1,4-DHP could come up to 94.42% after 100 min irradiation, which is much higher than Na-CDs (33.31%), Fe-CDs (76.86%), Cu-CDs (56.38%) and 250-FeCu-CDs (43.66%). The photooxidation reaction rate of CDs was further analysed by plotting the ln (A_t/A_0) − t curves (Fig. S9e-f). The slope (k) of the photooxidation with 350-FeCu-CDs is 0.0275 min^{-1}, which is also much higher than single metal doping CDs and 250-FeCu-CDs (Table S2). In addition, the photostabilities of 350-FeCu-CDs and 1,4-DHP were separately investigated by UV–Vis absorption spectra (Fig. S10). These results indicate that these CDs are stable and the higher graphitization degree and synergistic action of co-metal dopants (at 350 °C) could effectively enhance the photocatalytic ability.

3.4. Photocatalytic mechanism investigation

In order to further explore the role of electron transfer in the photocatalysis, the ESR spectra were used to explore the photocatalytic mechanism (Fig. S11 and Fig. 3d). 5,5-dimethyl-1-pyrroline-N-oxide (DMPO) was used as trapping agent for superoxide radical anion ($O_2^{-\bullet}$). When 1,4-DHP, FeCu-CDs and DMPO were mixed together in aqueous solution, the ESR signal attributed to $O_2^{-\bullet}$ adduct can be detected (Fig. 3d). As can be seen in Fig. 3d,

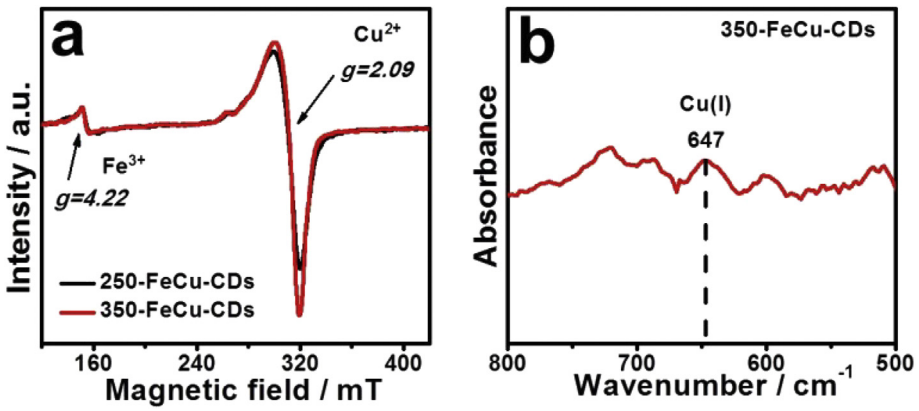

Fig. 2. (a) The ESR signals of Cu^{2+} and Fe^{3+} from FeCu-CDs; (b) the FT-IR spectra of 350-FeCu-CDs. (A colour version of this figure can be viewed online.)

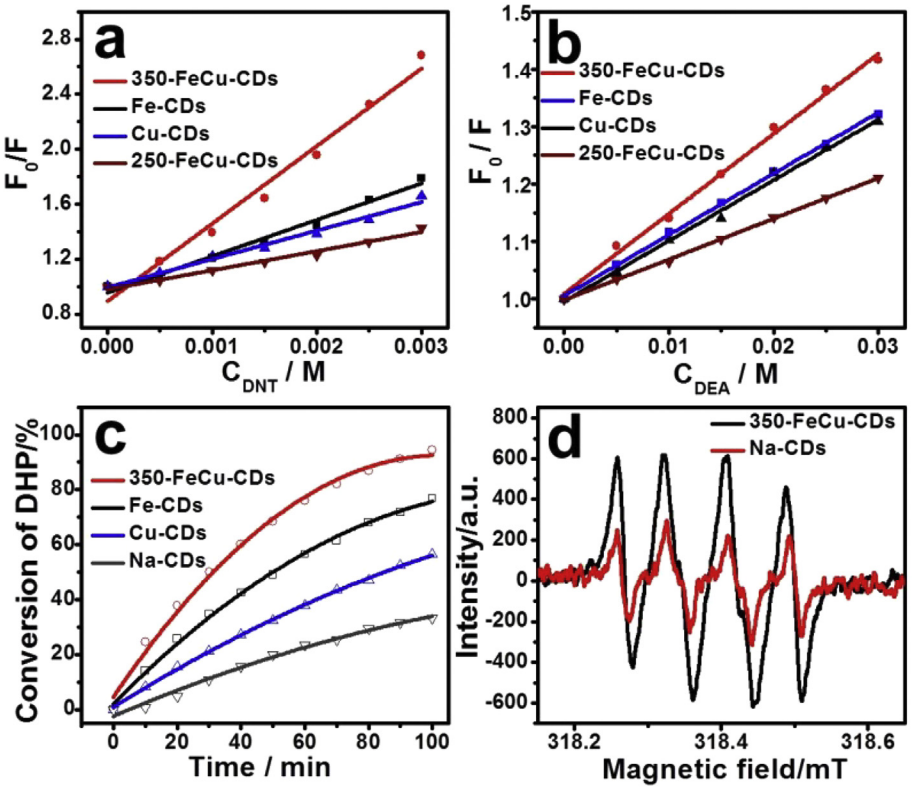

Fig. 3. (a) Stern-Volmer plot of the emission intensity of different CDs with various amounts of DNT upon excitation at 350 nm; (b) Stern-Volmer plot of the emission intensity of different CDs with various amounts of DEA upon excitation at 350 nm; (c) The conversion rate of 1,4-DHP catalyzed by different CDs; (d) The ESR signals of 350-FeCu-CDs and Na-CDs, with 1,4-DHP (1.0×10^{-4} M) and DMPO (1.0×10^{-2} M), irradiated for 12 min. (A colour version of this figure can be viewed online.)

the ability to produce $O_2^{-\bullet}$ of 350-FeCu-CDs is better than that of Na-CDs, which could explain the better performance of 350-FeCu-CDs for the photooxidation of 1,4-DHP. In the absence of 1,4-DHP or 350-FeCu-CDs, no $O_2^{-\bullet}$ signal was detected (Fig. S11a-b). It indicates that there is a unique electron transfer (1,4-DHP → FeCu-CDs → O_2) [14,15].

During this electron transfer process, FeCu-CDs, especially for their Fe and Cu dopants chelated with the graphene structure, play as electron acceptor and electron donor in the photocatalysis. For CDs samples with only Cu doping (Cu-CDs) or Fe doping (Fe-CDs), it is difficult to tune the Cu or Fe valence state (Fig. S12a-b). Therefore, the co-doping of Cu and Fe was critical in this photooxidation process. To further confirm the interactions between Fe and Cu species, ESR spectra were measured to further reveal the valance-state change during the electron transfer process (Fig. 4a–b). When 350-FeCu-CDs and 1,4-DHP mixed together in the absence of oxygen, there were both Fe^{3+} and Cu^{2+} signals (Fig. 4a–b). After irradiating for 30 min, both of Fe^{3+} and Cu^{2+} signals became weak. It indicates that Fe^{3+} and Cu^{2+} could react with 1,4-DHP and generate the Fe^{2+} and Cu^{+} (no ESR signal), which can explain electron maybe transfer from 1,4-DHP to the Fe and Cu dopants (Fe^{2+} and Cu^{+}) in 350-FeCu-CDs, and produce the CD radical ($CDs^{-\bullet}$) and the 1,4-DHP radical cation ($1,4\text{-}DHP^{+\bullet}$). As contrast, ESR spectra of Fe^{3+} and Cu^{2+} were obtained in the presence of oxygen (Fig. S13). After irradiating for 30 min, both of Fe^{3+} and Cu^{2+} signals became weak. However, both of Fe^{3+} and Cu^{2+} signals gradually recovered after 30 min irradiation. It indicated that electron transfer from 1,4-DHP to CDs was faster than that from CDs to O_2. When 1,4-DHP was gradually consumed after 30 min, electron transfer from CDs to O_2 came to the major role, so Fe^{3+} and Cu^{2+} signals gradually recovered. Then $1,4\text{-}DHP^{+\bullet}$ can release H^+ and its electron transfers to molecular oxygen under air atmosphere, generating an aromatization product of 1,4-DHP. Subsequently, reactive oxygen radical ($O_2^{\bullet}$) competes with the photosensitizer $CDs^{-\bullet}$ ($O_2^{\bullet} + Fe^{2+} \rightarrow O_2^{-\bullet} + Fe^{3+}$, $O_2^{\bullet} + Cu^{+} \rightarrow O_2^{-\bullet} + Cu^{2+}$) to form superoxide anion radical ($O_2^{-\bullet}$) and FeCu-CDs anion restore the ground state. Finally, $O_2^{-\bullet}$ reacts with H^+ to produce H_2O_2 (Fig. 4c). H_2O_2 is subsequently decomposed into O_2 and H_2O with the help of CDs [46], being in accordance with the demands of green chemistry by producing environmentally friendly side products. In order to better demonstrate the role of unsaturated metal dopants with mixed valence states, the simplified mechanism diagram was shown in Fig. S14. Mixed valence-metal doping CDs can enhance both the electron donating/accepting abilities and further improve the photocatalytic ability. With the help of graphene structure, Fe and Cu dopants could easily get electron from the reaction substrate (1,4-DHP) and transfer the electron to another substrate (O_2). In another words, these unsaturated dopants also promote the electron transfer in the photocatalysis.

4. Conclusion

In summary, under different temperature, FeCu-CDs with various graphitization degree were prepared by one-step pyrolysis. The graphitization degree of FeCu-CDs was proved by means of TEM, Raman, XRD and XPS spectra. Compared to 250-FeCu-CDs, 350-FeCu-CDs exhibit a higher graphitization degree which benefits the electron transfer in the photooxidation. These graphene structures promote the formation of unsaturated metal dopants with mixed valence states (Cu^{2+}, Cu^{+}, Fe^{3+}, Fe^{2+}), which were proved by XPS, ESR and FT-IR spectra. In another way, these unsaturated metal dopants perform the valence states change in the

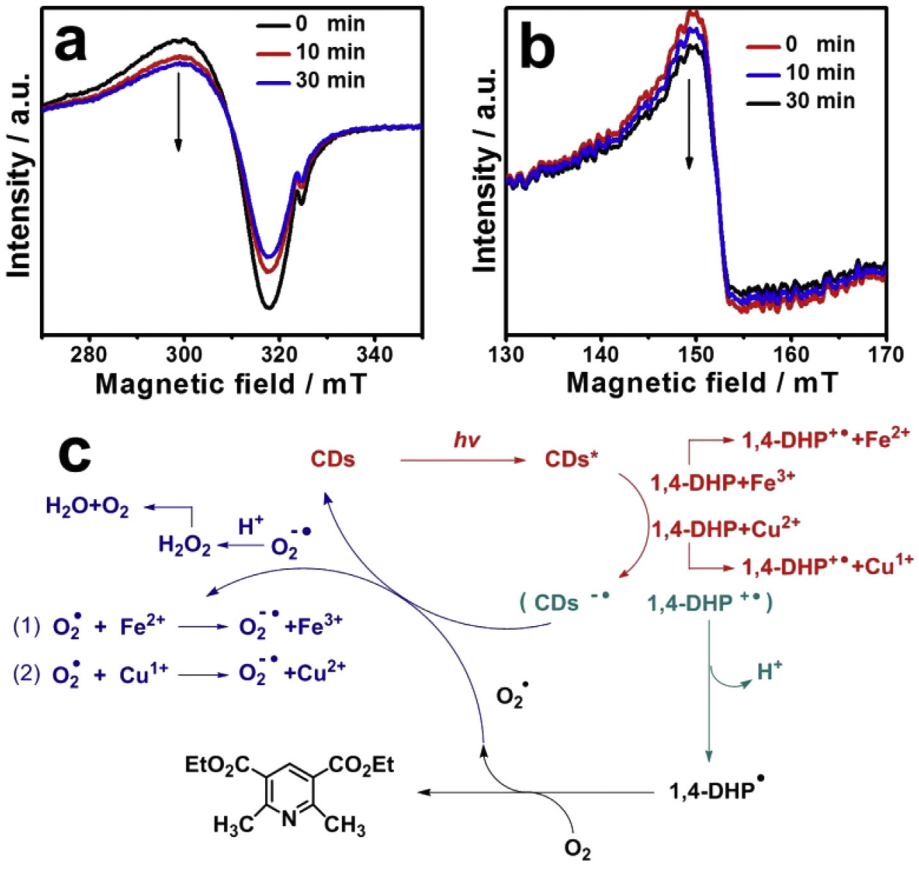

Fig. 4. (a) The ESR signals of Cu^{2+} of 350-FeCu-CDs with 1,4-DHP at 77 K, in the absence of oxygen; (b) The ESR signals of Fe^{3+} of 350-FeCu-CDs with 1,4-DHP at 77 K, in the absence of oxygen; (c) Mechanism for the photooxidation of 1,4-DHP with superoxide radical anion ($O_2^{-\bullet}$). (A colour version of this figure can be viewed online.)

photocatalysis, and they are beneficial to enhance both the electron donating/accepting abilities and further to improve the photocatalytic ability. Based on the excellent properties, FeCu-CDs prepared at high temperature have more graphene structures and show excellent catalytic activity for the photooxidation of 1,4-DHP. The reaction rate of 1,4-DHP catalyzed by 350-FeCu-CDs is 8 times higher than that of Na-CDs.

Acknowledgments

This work was financially supported by NSFC (51672309, 21302224, 51172285, 51372277, 21406269 and 21572269), Shandong Provincial Key Research Program (2015GSF121017), Project of Science and Technology Program for Basic Research of Qingdao (14-2-4-47-jch) and the Fundamental Research Funds for Central Universities (15CX05010A, 15CX08005A and 15CX05013A).

Appendix A. Supplementary data

Supplementary data related to this article can be found at https://doi.org/10.1016/j.carbon.2017.10.006.

References

[1] T.F. Yeh, S.J. Chen, H. Teng, Synergistic effect of oxygen and nitrogen functionalities for graphene-based quantum dots used in photocatalytic H_2 production from water decomposition, Nano Energy 12 (2015) 476–485.
[2] H. Yu, Y. Zhao, C. Zhou, L. Shang, Y. Peng, Y. Cao, et al., Carbon quantum dots/TiO_2 composites for efficient photocatalytic hydrogen evolution, J. Mater. Chem. A 2 (10) (2014) 3344–3351.
[3] J. Tian, Y. Leng, Z. Zhao, Y. Xia, Y. Sang, P. Hao, et al., Carbon quantum dots/hydrogenated TiO2 nanobelt heterostructures and their broad spectrum photocatalytic properties under UV, visible, and near-infrared irradiation, Nano Energy 11 (2015) 419–427.
[4] B.C. Martindale, G.A. Hutton, C.A. Caputo, E. Reisner, Solar hydrogen production using carbon quantum dots and a molecular nickel catalyst, J. Am. Chem. Soc. 137 (18) (2015) 6018–6025.
[5] T.F. Yeh, C.Y. Teng, S.J. Chen, H. Teng, Nitrogen-doped graphene oxide quantum dots as photocatalysts for overall water-splitting under visible light illumination, Adv. Mater. 26 (20) (2014) 3297–3303.
[6] L. Cao, S. Sahu, P. Anilkumar, C.E. Bunker, J. Xu, K.A. Fernando, et al., Carbon nanoparticles as visible-light photocatalysts for efficient CO2 conversion and beyond, J. Am. Chem. Soc. 133 (13) (2011) 4754–4757.
[7] A. Fujishima, Electrochemical photolysis of water at a semiconductor electrode, nature 238 (5358) (1972) 37–38.
[8] K.A. Fernando, S. Sahu, Y. Liu, W.K. Lewis, E.A. Guliants, A. Jafariyan, et al., Carbon quantum dots and applications in photocatalytic energy conversion, ACS Appl. Mater Interfaces 7 (16) (2015) 8363–8376.
[9] T. Hisatomi, J. Kubota, K. Domen, Recent advances in semiconductors for photocatalytic and photoelectrochemical water splitting, Chem. Soc. Rev. 43 (22) (2014) 7520–7535.
[10] H. Tetsuka, R. Asahi, A. Nagoya, K. Okamoto, I. Tajima, R. Ohta, et al., Optically tunable amino-functionalized graphene quantum dots, Adv. Mater. 24 (39) (2012) 5333–5338.
[11] H. Li, X. He, Z. Kang, H. Huang, Y. Liu, J. Liu, et al., Water-soluble fluorescent carbon quantum dots and photocatalyst design, Angew. Chem. Int. Ed. 49 (26) (2010) 4430–4434.
[12] H. Yu, R. Shi, Y. Zhao, G.I. Waterhouse, L.Z. Wu, C.H. Tung, et al., Smart utilization of carbon dots in semiconductor photocatalysis, Adv. Mater. 28 (43) (2016) 9454–9477.
[13] X. Wang, L. Cao, F. Lu, M.J. Meziani, H. Li, G. Qi, et al., Photoinduced electron transfers with carbon dots, Chem. Commun. 46 (25) (2009) 3774–3776.
[14] X. Shao, W. Wu, R. Wang, J. Zhang, Z. Li, Y. Wang, et al., Engineering surface structure of petroleum-coke-derived carbon dots to enhance electron transfer for photooxidation, J. Catal. 344 (2016) 236–241.
[15] W. Wu, L. Zhan, W. Fan, J. Song, X. Li, Z. Li, et al., Cu-N dopants boost electron transfer and photooxidation reactions of carbon dots, Angew. Chem. Int. Ed. 54 (22) (2015) 6540–6544.
[16] P. Yu, X. Wen, Y.-R. Toh, Y.-C. Lee, K.-Y. Huang, S. Huang, et al., Efficient electron transfer in carbon nanodot–graphene oxide nanocomposites,

J. Mater. Chem. C 2 (16) (2014) 2894–2901.
[17] Q.H. Wang, Z. Jin, K.K. Kim, A.J. Hilmer, G.L. Paulus, C.J. Shih, et al., Understanding and controlling the substrate effect on graphene electron-transfer chemistry via reactivity imprint lithography, Nat. Chem. 4 (9) (2012) 724–732.
[18] G.L. Paulus, Q.H. Wang, M.S. Strano, Covalent electron transfer chemistry of graphene with diazonium salts, Acc. Chem. Res. 46 (1) (2013) 160–170.
[19] M. Velický, D.F. Bradley, A.J. Cooper, E.W. Hill, I.A. Kinloch, A. Mishchenko, et al., Electron transfer kinetics on mono- and multilayer graphene, ACS Nano 8 (10) (2014) 10089–10100.
[20] A. Indra, A. Acharjya, P.W. Menezes, C. Merschjann, D. Hollmann, M. Schwarze, et al., Boosting visible-light-driven photocatalytic hydrogen evolution with an integrated nickel phosphide-carbon nitride system, Angew. Chem. Int. Ed. 56 (6) (2017) 1653–1657.
[21] G. Qi, J. Xu, J. Su, J. Chen, X. Wang, F. Deng, Low-temperature reactivity of Zn+ ions confined in ZSM-5 zeolite toward carbon monoxide oxidation: insight from in situ DRIFT and ESR spectroscopy, J. Am. Chem. Soc. 135 (18) (2013) 6762–6765.
[22] Y.K. Hwang, D.Y. Hong, J.S. Chang, S.H. Jhung, Y.K. Seo, J. Kim, et al., Amine grafting on coordinatively unsaturated metal centers of MOFs: consequences for catalysis and metal encapsulation, Angew. Chem. Int. Ed. 47 (22) (2008) 4144–4148.
[23] Q. Fu, W.X. Li, Y. Yao, H. Liu, H.Y. Su, D. Ma, et al., Interface-confined ferrous centers for catalytic oxidation, Science 328 (5982) (2010) 1141–1144.
[24] W. Tu, Y. Zhou, Z. Zou, Versatile graphene-promoting photocatalytic performance of semiconductors: basic principles, synthesis, solar energy conversion, and environmental applications, Adv. Funct. Mater. 23 (40) (2013) 4996–5008.
[25] D. Zhang, L.Z. Wu, L. Zhou, X. Han, Q.Z. Yang, L.P. Zhang, et al., Photocatalytic hydrogen production from hantzsch 1,4-dihydropyridines by platinum(II) terpyridyl complexes in homogeneous solution, J. Am. Chem. Soc. 126 (11) (2004) 3440–3441.
[26] T. Chenho, Photooxidation of Hantzsch 1,4-dihydropyridines by molecular oxygen, Chin. Sci. Bull. 55 (25) (2010) 2855–2858.
[27] P. Prakash, E. Gravel, H. Li, F. Miserque, A. Habert, M.D. Hertog, et al., Direct and co-catalytic oxidative aromatization of 1,4-dihydropyridines and related substrates using gold nanoparticles supported on carbon nanotubes, Catal. Sci. Technol. 6 (17) (2016) 6476–6479.
[28] B. Vacher, B. Bonnaud, P. Funes, N. Jubault, W. Koek, M.B. Assié, et al., Novel derivatives of 2-pyridinemethylamine as selective, potent, and orally active agonists at 5-HT1A receptors, J. Med. Chem. 42 (9) (1999) 1648–1660.
[29] W.W. Zhang, Y.B. Chen, W.D. Chen, Z.W. Liu, Z. Li, Designing tetrahydroimidazo[1,2-a]pyridine derivatives via catalyst-free aza-Diels-Alder reaction (ADAR) and their insecticidal evaluation, J. Agric. Food. Chem. 58 (10) (2010) 6296–6299.
[30] H. Huang, H. Hu, S. Qiao, L. Bai, M. Han, Y. Liu, et al., Carbon quantum dot/CuSx nanocomposites towards highly efficient lubrication and metal wear repair, Nanoscale 7 (26) (2015) 11321–11327.
[31] J. Liu, W. Zhu, S. Yu, X. Yan, Three dimensional carbogenic dots/TiO_2 nano-heterojunctions with enhanced visible light-driven photocatalytic activity, Carbon 79 (2014) 369–379.
[32] Y. Dong, H. Pang, H.B. Yang, C. Guo, J. Shao, Y. Chi, et al., Carbon-based dots co-doped with nitrogen and sulfur for high quantum yield and excitation-independent emission, Angew. Chem. Int. Ed. 52 (30) (2013) 7800–7804.
[33] Y. Guo, J. Li, Y. Yuan, L. Li, M. Zhang, C. Zhou, et al., A rapid microwave-assisted thermolysis route to highly crystalline carbon nitrides for efficient hydrogen generation, Angew. Chem. Int. Ed. 55 (47) (2016) 14693–14697.
[34] D. Qu, M. Zheng, P. Du, Y. Zhou, L. Zhang, D. Li, et al., Highly luminescent S, N co-doped graphene quantum dots with broad visible absorption bands for visible light photocatalysts, Nanoscale 5 (24) (2013) 12272–12277.
[35] D. Dey, T. Bhattacharya, B. Majumdar, S. Mandani, B. Sharma, T.K. Sarma, Carbon dot reduced palladium nanoparticles as active catalysts for carbon-carbon bond formation, Dalton Trans. 42 (38) (2013) 13821–13825.
[36] M. Wu, Y. Wang, W. Wu, C. Hu, X. Wang, J. Zheng, et al., Preparation of functionalized water-soluble photoluminescent carbon quantum dots from petroleum coke, Carbon 78 (2014) 480–489.
[37] Z. Ma, H. Ming, H. Huang, Y. Liu, Z. Kang, One-step ultrasonic synthesis of fluorescent N-doped carbon dots from glucose and their visible-light sensitive photocatalytic ability, New J. Chem. 36 (4) (2012) 861–864.
[38] P. Chen, T.Y. Xiao, Y.H. Qian, S.S. Li, S.H. Yu, A nitrogen-doped graphene/carbon nanotube nanocomposite with synergistically enhanced electrochemical activity, Adv. Mater. 25 (23) (2013) 3192–3196.
[39] Z. Li, H. Yu, T. Bian, Y. Zhao, C. Zhou, L. Shang, et al., Highly luminescent nitrogen-doped carbon quantum dots as effective fluorescent probes for mercuric and iodide ions, J. Mater. Chem. C 3 (9) (2015) 1922–1928.
[40] Q. Liu, T. Chen, Y. Guo, Z. Zhang, X. Fang, Grafting Fe(III) species on carbon nanodots/Fe-doped g-C3N4 via interfacial charge transfer effect for highly improved photocatalytic performance, Appl. Catal. B 205 (2017) 173–181.
[41] W.L. And, H. Frei, Photochemical CO2 splitting by metal-to-metal charge-transfer excitation in mesoporous ZrCu(I)-MCM-41 silicate sieve, J. Am. Chem. Soc. 127 (6) (2005) 1610–1611.
[42] T. Yamashita, P. Hayes, Analysis of XPS spectra of Fe2+ and Fe3+ ions in oxide materials, Appl. Surf. Sci. 254 (8) (2008) 2441–2449.
[43] P. Jiang, D. Prendergast, F. Borondics, S. Porsgaard, L. Giovanetti, E. Pach, et al., Experimental and theoretical investigation of the electronic structure of Cu_2O and CuO thin films on Cu(110) using x-ray photoelectron and absorption spectroscopy, J. Chem. Phys. 138 (2) (2013) 024704.
[44] Z. Hussain, M.A. Salim, M.A. Khan, E.E. Khawaja, X-ray photoelectron and auger spectroscopy study of copper-sodium-germanate glasses, J. Non-Cryst. Solids 110 (1) (1989) 44–52.
[45] J. Ghijsen, L.H. Tjeng, J. van Elp, H. Eskes, J. Westerink, G.A. Sawatzky, et al., Electronic structure ofCu_2O and CuO, Phys. Rev. B 38 (16) (1988) 11322–11330.
[46] J. Liu, Y. Liu, N. Liu, Y. Han, X. Zhang, H. Huang, et al., Water splitting. Metal-free efficient photocatalyst for stable visible water splitting via a two-electron pathway, Science 347 (6225) (2015) 970–974.